Unidirectional reflectionless propagation in plasmonic waveguide-cavity systems at exceptional points

Yin Huang,[1,2,*] Georgios Veronis,[3,4] and Changjun Min[5]

[1]*Department of Optoelectrics Information Science and Engineering, School of Physics and Electronics, Central South University, Changsha, Hunan 410012, China*
[2]*Institute of Super-microstructure and Ultrafast Process in Advanced Materials and Hunan Key Laboratory for Super-microstructure and Ultrafast Process, School of Physics and Electronics, Central South University, Changsha, Hunan 410083, China*
[3]*School of Electrical Engineering and Computer Science, Louisiana State University, Baton Rouge, Louisiana 70803, USA*
[4]*Center for Computation and Technology, Louisiana State University, Baton Rouge, Louisiana 70803, USA*
[5]*Institute of Micro-Nano Optics, Key Laboratory of Optoelectronic Devices and Systems of Ministry of Education and Guangdong Province, College of Optoelectronic Engineering, Shenzhen University, Shenzhen 518060, China*

[*]*yhuan15@csu.edu.cn*

Abstract: We design a non-parity-time-symmetric plasmonic waveguide-cavity system, consisting of two metal-dielectric-metal stub resonators side coupled to a metal-dielectric-metal waveguide, to form an exceptional point, and realize unidirectional reflectionless propagation at the optical communication wavelength. The contrast ratio between the forward and backward reflection almost reaches unity. We show that the presence of material loss in the metal is critical for the realization of the unidirectional reflectionlessness in this plasmonic system. We investigate the realized exceptional point, as well as the associated physical effects of level repulsion, crossing and phase transition. We also show that, by periodically cascading the unidirectional reflectionless plasmonic waveguide-cavity system, we can design a wavelength-scale unidirectional plasmonic waveguide perfect absorber. Our results could be potentially important for developing a new generation of highly compact unidirectional integrated nanoplasmonic devices.

OCIS codes: (240.6680) Surface plasmons; (260.3910) Metal optics; (130.2790) Guided waves.

References and links

1. K. G. Makris, R. EI-Ganainy, D. N. Christodoulides, and Z. H. Musslimani, "Beam dynamics in *PT* symmetric optical lattices," Phys. Rev. Lett. **100**, 103904 (2008).
2. Z. H. Musslimani, K. G. Makris, R. El-Ganainy, and D. N. Christodoulides, "Optical solitons in *PT* periodic potentials," Phys. Rev. Lett. **100**, 030402 (2008).
3. C. E. Ruter, K. G. Makris, R. El-Ganainy, D. N. Christodoulides, M. Segev, and D. Kip, "Observation of parity-time symmetry in optics," Nat. Phys. **6**, 192–195 (2010).
4. A. Guo, G. J. Salamo, D. Duchesne, R. Morandotti, M. Volatier-Ravat, V. Aimez, G. A. Siviloglou, and D. N. Christodoulides, "Observation of *PT*-symmetry breaking in complex optical potentials," Phys. Rev. Lett. **103**, 093902 (2009).

#247970 Received 20 Aug 2015; revised 30 Oct 2015; accepted 3 Nov 2015; published 6 Nov 2015

5. B. Peng, S. K. Ozdemir, F. Lei, F. Monifi, M. Gianfreda, G. L. Long, S. Fan, F. Nori, C. M. Bender, and L. Yang, "Parity-time-symmetric whispering gallery microcavities," Nat. Phys. **10**, 394–398 (2014).
6. S. Longhi, "*PT*-symmetric laser absorber," Phys. Rev. A **82**, 031801 (2010).
7. Y. D. Chong, L. Ge, and A. D. Stone, "*PT*-symmetry breaking and laser-absorber modes in optical scattering systems," Phys. Rev. Lett. **106**, 093902 (2011).
8. Y. Sun, W. Tan, H. Li, J. Li, and H. Chen, "Experimental demonstration of a coherent perfect absorber with *PT* phase transition," Phys. Rev. Lett. **112**, 143903 (2014).
9. L. Chang, X. Jiang, S. Hua, C. Yang, J. Wen, L. Jiang, G. Li, G. Wang and M. Xiao, "Parity-time symmetry and variable optical isolation in active-passive-coupled microresonators," Nat. Photonics **8**, 524–529 (2014).
10. S. V. Dmitriev, A. A. Sukhorukov, and Y. S. Kivshar, "Binary parity-time-symmetric nonlinear lattices with balanced gain and loss," Opt. Lett. **35**, 2976–2978 (2010).
11. N. Lazarides and G. P. Tsironis, "Gain-driven discrete breathers in *PT*-symmetric nonlinear metamaterials," Phys. Rev. Lett. **110**, 053901 (2013).
12. W. D. Heiss, "Exceptional points of non-Hermitian operators," J. Phys. Math. Gen. **37**, 2455–2464 (2004).
13. W. D. Heiss, "Repulsion of resonance states and exceptional points," Phys. Rev. E **61**, 929–932 (2000).
14. Q. H. Song and H. Cao, "Improving optical confinement in nanostructures via external mode coupling," Phys. Rev. Lett. **105**, 053902 (2010).
15. S. Y. Lee, J. W. Ryu, S. W. Kim, and Y. Chung, "Geometric phase around multiple exceptional points," Phys. Rev. A **85**, 064103 (2012).
16. Z. Lin, H. Ramezani, T. Eichelkraut, T. Kottos, H. Cao, and D. N. Christodoulides, "Unidirectional invisibility induced by *PT*-symmetric periodic structures," Phys. Rev. Lett. **106**, 213901 (2011).
17. A. Regensburger, C. Bersch, M. A. Miri, G. Onishchukov, D. N. Christodoulides, and U. Peschel, "Parity-time synthetic photonic lattices," Nature **488**, 167–171 (2012).
18. L. Ge, Y. D. Chong, and A. D. Stone, "Conservation relations and anisotropic transmission resonances in one-dimensional *PT*-symmetric photonic heterostructures," Phys. Rev. A **85**, 023802 (2012).
19. J. Gear, F. Liu, S. T. Chu, S. Rotter, and J. Li, "Parity-time symmetry from stacking purely dielectric and magnetic slabs," Phys. Rev. A **91**, 033825 (2015).
20. L. Feng, Y. L. Xu, W. S. Fegadolli, M. H. Lu, J. E. B. Oliveira, V. R. Almeida, Y. F. Chen, and A. Scherer, "Experimental demonstration of a unidirectional reflectionless parity-time metamaterial at optical frequencies," Nat. Mater. **12**, 108–113 (2013).
21. J. Wu, M. Artoni, and G. C. La Rocca, "Non-Hermitian degeneracies and unidirectional reflectionless atomic lattices," Phys. Rev. Lett. **113**, 123004 (2014).
22. S. A. R. Horsley, M. Artoni, and G. C. La Rocca, "Spatial Kramer-Kronig relations and the reflection of waves," Nat. Photonics **9**, 436–439 (2015).
23. S. Yu, X. Piao, K.W. Yoo, J. Shin, and N. Park, "One-way optical modal transition based on causality in momentum space," Opt. Express **23**, 24997–25008 (2015).
24. X. Yin and X. Zhang, "Unidirectional light propagation at exceptional points," Nat. Mater. **12**, 175–177 (2013).
25. L. Feng, X. Zhu, S. Yang, H. Zhu, P. Zhang, X. Yin, Y. Wang, and X. Zhang, "Demonstration of a large-scale optical exceptional point structure," Opt. Express **22**, 1760–1767 (2014).
26. Y. Shen, X. Hua Deng, and L. Chen, "Unidirectional invisibility in a two-layer non-*PT*-symmetric slab," Opt. Express **22**, 19440–19447 (2014).
27. W. L. Barnes, A. Dereux, and T. W. Ebbesen, "Surface plasmon subwavelength optics," Nature (London) **424**, 824–830 (2003).
28. C. Min and G. Veronis, "Absorption switches in metal-dielectric-metal plasmonic waveguides," Opt. Express **16,** 10757–10766 (2009).
29. L. Yang, C. Min, and G. Veronis, "Guided subwavelength slow-light mode supported by a plasmonic waveguide system," Opt. Lett. **35,** 4184–4186 (2010).
30. J. Nath, S. Modak, I. Rezadad, D. Panjwani, F. Rezaie, J. W. Cleary, and R. E. Peale, "Far-infrared absorber based on standing-wave resonances in metal-dielectric-metal cavity," Opt. Express **23,** 20366–20380 (2015).
31. G. Cao, H. Li, Y. Deng, S. Zhan, Z. He, and B. Li, "Plasmon-induced transparency in a single multimode stub resonator," Opt. Express **22,** 25215–25223 (2014).
32. Y. Huang, C. Min, P. Dastmalchi, and G. Veronis, "Slow-light enhanced subwavelength plasmonic waveguide refractive index sensors," Opt. Express **23,** 14922–14936 (2015).
33. S. Zhan, H. Li, Z. He, B. Li, Z. Chen, and H. Xu, "Sensing analysis based on plasmon induced transparency in nanocavity-coupled waveguide," Opt. Express **23,** 20313–20320 (2015).
34. I. Zand, A. Mahigir, T. Pakizeh, and M. S. Abrishamian, "Selective-mode optical nanofilters based on plasmonic complementary split-ring resonators," Opt. Express **20,** 7516–7525 (2012).
35. Y. Huang, C. Min, and G. Veronis, "Subwavelength slow-light waveguides based on a plasmonic analogue of electromagnetically induced transparency," Appl. Phys. Lett. **99,** 143117 (2011).
36. E. N. Economou, "Surface plasmons in thin films," Phys. Rev. **182,** 539–554 (1969).
37. J. A. Dionne, H. J. Lezec, and H. A. Atwater, "Highly confined photon transport in subwavelength metallic slot waveguides," Nano Lett. **6,** 1928–1932 (2006).

#247970 Received 20 Aug 2015; revised 30 Oct 2015; accepted 3 Nov 2015; published 6 Nov 2015

38. P. Neutens, P. Van Dorpe, I. De Vlaminck, L. Lagae, and G. Borghs, "Electrical detection of confined gap plasmons in metal-insulator-metal waveguides," Nat. Photonics **3,** 283–286 (2009).
39. C. M. Bender and S. Boettcher, "Real spectra in non-Hermitian Hamiltonians having *PT* symmetry," Phys. Rev. Lett. **80**, 5243–5246 (1998).
40. G. Veronis, R. W. Dutton, and S. Fan, "Method for sensitivity analysis of photonic crystal devices," Opt. Lett. **29,** 2288–2290 (2004).
41. E. D. Palik, *Handbook of Optical Constants of Solids* (Academic, 1985).
42. J. Jin, *The Finite Element Method in Electromagnetics* (Wiley, 2002).
43. Y. Huang, C. Min, and G. Veronis, "Compact slit-based couplers for metal-dielectric-metal plasmonic waveguides," Opt. Express **20,** 22233–22244 (2012).
44. S. E. Kocabas, G. Veronis, D. A. B. Miller, and S. Fan, "Transmission line and equivalent circuit models for plasmonic waveguide components," IEEE J. Sel. Topics Quantum Electron. **14,** 1462–1472 (2008).
45. Y. Choi, S. Kang, S. Lim, W. Kim, J. R. Kim, J. H. Lee, and K. An, "Quasieigenstate coalescence in an atom-cavity quantum composite," Phys. Rev. Lett. **104**, 153601 (2010).
46. H. Cartarius, J. Main, and G. Wunner, "Exceptional points in atomic spectra," Phys. Rev. Lett. **99**, 173003 (2007).
47. J. D. Jackson, *Classical Electrodynamics* (Wiley, 1998).
48. S. Yu, X. Piao, J. Hong, and N. Park, "Progress toward high-Q perfect absorption: A Fano antilaser," Phys. Rev. A **92**, 011802 (2015).
49. S. Longhi, "Non-reciprocal transmission in photonic lattices based on unidirectional coherent perfect absorption," Opt. Lett. **40,** 1278–1281 (2015).
50. J. R. Piper and S. Fan, "Total absorption in a graphene monolayer in the optical regime by critical coupling with a photonic crystal guided resonance," ACS Photon. **1**, 347–353 (2014).
51. W. Shin, W. Cai, P. B. Catrysse, G. Veronis, M. L. Brongersma, and S. Fan, "Broadband sharp 90-degree bends and T-splitters in plasmonic coaxial waveguides," Nano Lett. **13,** 4753–4758 (2013).
52. A. Mahigir, P. Dastmalchi, W. Shin, S. Fan, and G. Veronis, "Plasmonic coaxial waveguide-cavity devices," Opt. Express **23,** 20549–20562 (2015).

1. Introduction

In the past few years, parity-time (*PT*) symmetric optical systems have attracted considerable attention because they provide a route to study the physics of non-Hermitian Hamiltonians. The constructed *PT*-symmetric optical structures can lead to a range of extraordinary phenomena, including novel beam refraction [1], power oscillation [2, 3], loss-induced transparency [4], nonreciprocal light transmission [3, 5], perfect absorption [6–8], optical isolation [9], and various other novel nonlinear effects [10, 11]. Exceptional points, which are branch point singularities of the spectrum, associated with the coalescence of both eigenvalues and corresponding eigenstates, lead to interesting phenomena such as level repulsion and crossing, bifurcation, chaos, and phase transitions in open quantum systems described by non-Hermitian Hamiltonians [12–15]. Recently, there has been significant progress in using *PT*-symmetric periodic optical structures with balanced gain and loss to attain unidirectional light reflectionlessness. In such structures the reflection is zero when measured from one end of the structure at exceptional points, and nonzero when measured from the other end [16–18]. In addition, Gear *et al.* demonstrated unidirectional reflectionlessness in a *PT*-symmetric optical structure with alternating purely dielectric and purely magnetic slabs [19]. Unidirectional light reflectionlessness can also be attained in non-*PT*-symmetric structures [20–23]. In particular, Feng *et al.* and Wu *et al.* achieved unidirectional light reflection in easier to fabricate structures without gain media [20, 21]. This is due to the fact that exceptional points exist in a larger family of non-Hermitian Hamiltonians [24]. Thus, asymmetric light propagation can be observed in both *PT*-synthetic materials possessing active (gain) media, as well as in passive (lossy) systems, in which the optical *PT* symmetry is therefore broken. Most recently, Feng *et al.* demonstrated unidirectional reflectionless light transport at the exceptional point in a conventional large-size non-periodic multilayer structure consisting of lossy and lossless dielectrics [25]. Finally, Shen *et al.* showed theoretically that such a unidirectional phenomenon can be realized in a similar two-layer non-*PT*-symmetric slab structure [26].

Plasmonic waveguides have shown the potential to guide and manipulate light at deep sub-

#247970 Received 20 Aug 2015; revised 30 Oct 2015; accepted 3 Nov 2015; published 6 Nov 2015

wavelength scales [27]. Among different plasmonic waveguiding structures, metal-dielectric-metal (MDM) plasmonic waveguides, which are the optical analogue of microwave two-conductor transmission lines [28], are of particular interest [28–35], because they support modes with deep subwavelength scale over a very wide range of frequencies extending from DC to visible [36], and are relatively easy to fabricate [37, 38]. Achieving unidirectional reflectionless propagation in a MDM plasmonic waveguide system could be potentially important for developing a new generation of highly compact unidirectional integrated nanophotonic devices such as chip-scale optical network analyzers [17, 20].

In this paper, we introduce a non-*PT*-symmetric plasmonic waveguide-cavity system consisting of two MDM stub resonators side coupled to a MDM waveguide. In several previous studies periodic modulation of the refractive index profile, which requires careful tuning of the constituent materials, was used for synthesizing *PT*-symmetric optical structures [16-21]. Here, we instead tune the geometric parameters of the structure to obtain an exceptional point, and realize unidirectional reflectionlessness at the optical communication wavelength. The contrast ratio between the forward and backward reflection almost reaches unity. We show that the presence of material loss plays a crucial role on the realization of such a unidirectional phenomenon in the proposed plasmonic system. We investigate the properties of the realized exceptional point of the system, as well as the associated physical effects of level repulsion, crossing and phase transition. We also show that by properly cascading the plasmonic waveguide-cavity structures we can design a wavelength-scale unidirectional plasmonic waveguide perfect absorber.

The remainder of the paper is organized as follows. In Section 2, we employ single-mode scattering matrix theory to account for the behavior of the proposed plasmonic waveguide-cavity system. In Subsection 3.1 we use this theory to design a plasmonic waveguide system with unidirectional reflectionless propagation. The realized exceptional point of the system, as well as the associated physical effects of level repulsion, crossing and phase transition are then investigated in Subsection 3.2. In Subsection 3.3 we design a wavelength-scale unidirectional plasmonic waveguide perfect absorber by periodically cascading the unidirectional reflectionless structure which was designed in Subsection 3.1. Finally, our conclusions are summarized in Section 4.

2. Theory and design method

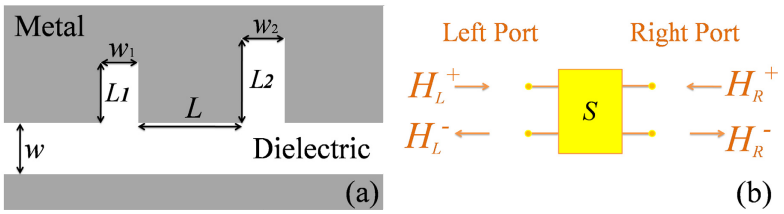

Fig. 1. (a) Schematic of a MDM plasmonic waveguide side coupled to two MDM stub resonators. (b) Scattering matrix **S** of the entire two-port plasmonic waveguide system of Fig. 1(a). H_L^+, and H_R^+ are the complex magnetic field amplitudes of the incoming modes at the left and right ports, respectively. Similarly, H_L^-, and H_R^- are the complex magnetic field amplitudes of the outgoing modes from the left and right ports, respectively.

Our proposed structure consists of two MDM stub resonators side coupled to a MDM waveguide [Fig. 1(a)]. Side-coupled-resonator structures have been previously proposed as compact filters, slow-light waveguides, switches and sensors for plasmonic waveguides [28, 29, 31–35]. The optical properties of our proposed system can be described by the scattering matrix **S** de-

#247970 Received 20 Aug 2015; revised 30 Oct 2015; accepted 3 Nov 2015; published 6 Nov 2015

fined by the following equation

$$\begin{pmatrix} H_R^- \\ H_L^- \end{pmatrix} = \mathbf{S} \begin{pmatrix} H_L^+ \\ H_R^+ \end{pmatrix} = \begin{pmatrix} t & r_b \\ r_f & t \end{pmatrix} \begin{pmatrix} H_L^+ \\ H_R^+ \end{pmatrix}, \tag{1}$$

where H_L^+, and H_R^+ are the complex magnetic field amplitudes of the incoming modes at the left and right ports, respectively. Similarly, H_L^-, and H_R^- are the complex magnetic field amplitudes of the outgoing modes from the left and right ports, respectively [Fig. 1(b)]. In addition, t is the complex transmission coefficient, while r_f, r_b are the complex reflection coefficients for light incident from the left (forward direction) and from the right (backward direction), respectively. In general, the matrix $\mathbf{S}$ is non-Hermitian, and its corresponding complex eigenvalues are $\lambda_s^{\pm} = t \pm \sqrt{r_f r_b}$. Its eigenstates, which are $\psi_{\pm} = (1, \pm\sqrt{\frac{r_f}{r_b}})^T$ for $r_b \neq 0$, are not orthogonal. It has been recognized that there is a close analogy between the Hamiltonian matrix in quantum mechanics and this optical scattering matrix [7, 16, 17, 25]. By engineering the Hamiltonian matrix in PT-symmetric quantum mechanical systems, its eigenvalue branches merge and PT symmetry breaks down with the appearance of exceptional points [3, 17, 39]. Similarly, in our proposed two-port plasmonic system (Fig. 1), by manipulating the elements of the scattering matrix, the two eigenvalues can be coalesced and form exceptional points. This leads to unidirectional reflectionless propagation in either the forward ($r_f = 0, r_b \neq 0$) or the backward direction ($r_b = 0, r_f \neq 0$).

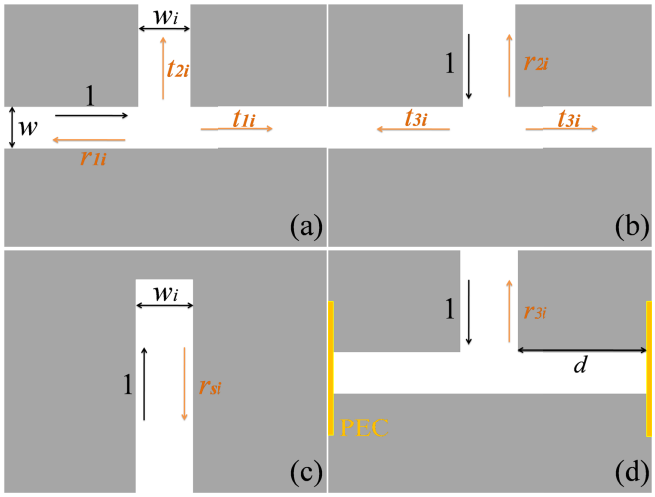

Fig. 2. (a) Schematic defining the reflection coefficient r_{1i}, and transmission coefficients t_{1i}, t_{2i}, when the fundamental TM mode of a MDM waveguide with width w is incident at a junction with a MDM waveguide with width w_i. (b) Schematic defining the reflection coefficient r_{2i}, and transmission coefficient t_{3i} when the fundamental TM mode of a MDM waveguide with width w_i is incident at a junction with a MDM waveguide with width w. (c) Schematic defining the reflection coefficient r_{si} of the fundamental TM mode of a MDM waveguide with width w_i at the boundary of a short-circuited MDM waveguide. (d) Schematic defining the reflection coefficient r_{3i} when the fundamental TM mode of a MDM waveguide with width w_i is incident at a junction with a MDM waveguide with width w which is terminated by perfect electric conductor (PEC) boundary conditions.

In the case of unidirectional reflectionless propagation in the forward direction ($r_f = 0, r_b \neq 0$), the scattering matrix $\mathbf{S}$ eigenvalues $\lambda_s^{\pm}$ coalesce into $\lambda_c = t$, and the eigenstates $\psi_{\pm}$ coalesce into the only eigenstate $\psi_c = (1,0)^T$. Since the scattering matrix eigenstates coalesce

#247970 Received 20 Aug 2015; revised 30 Oct 2015; accepted 3 Nov 2015; published 6 Nov 2015

into the only eigenstate $\psi_c = (1,0)^T$, they no longer form a complete basis [21]. We note that the eigenstate ψ_c corresponds, through Eq. (1), to a well defined physical scattering state with $(H_L^+, H_R^+)^T = \psi_c = (1,0)^T$ and $(H_R^-, H_L^-)^T = \lambda_c \psi_c = (t,0)^T$. In other words the eigenstate corresponds to a state with unidirectional reflectionless propagation for light incident from the left [21]. A similar discussion holds for the case of unidirectional reflectionless propagation in the backward direction ($r_b = 0, r_f \neq 0$).

Since the MDM waveguide and MDM stub resonators have deep subwavelength widths ($w, w_1, w_2 \ll \lambda$), only the fundamental TM mode is propagating. Thus, we can use single-mode scattering matrix theory to account for the behavior of the proposed system of Fig. 1(a) [32, 35]. The complex magnetic field reflection coefficients r_{1i}, r_{2i} and transmission coefficients t_{1i}, t_{2i}, t_{3i} for the fundamental propagating TM mode at a MDM waveguide junction are defined in Figs. 2(a) and 2(b), while the reflection coefficient at the boundary of a short-circuited MDM waveguide r_{si} is defined in Fig. 2(c). Alternatively, the transmission and reflection properties of our proposed system can also be described by the transfer matrix $\mathbf{T}$

$$\begin{pmatrix} H_R^- \\ H_R^+ \end{pmatrix} = \mathbf{T} \begin{pmatrix} H_L^+ \\ H_L^- \end{pmatrix}. \tag{2}$$

The transfer matrix for light propagating across the structure section containing stub resonator i can be calculated as

$$\mathbf{M}_i = \begin{pmatrix} \frac{b_i^2 - a_i^2}{b_i} & \frac{a_i}{b_i} \\ -\frac{a_i}{b_i} & \frac{1}{b_i} \end{pmatrix}, \tag{3}$$

where $a_i = r_{1i} + \frac{t_{2i}t_{3i}}{g_i - r_{2i}}, b_i = t_{1i} + \frac{t_{2i}t_{3i}}{g_i - r_{2i}}, g_i = \frac{e^{2\gamma_i L_i}}{r_{si}}$, L_i is the length of the ith MDM stub [Fig. 1(a)], and $\gamma_i = \alpha_i + j\beta_i$ is the complex wave vector of the fundamental propagating TM mode in the ith MDM stub. Therefore, the transfer matrix $\mathbf{T}$ of the entire system of the two MDM stubs coupled to the MDM waveguide [Fig. 1(a)] can be obtained by multiplying the transfer matrices of the individual components

$$\mathbf{T} = \mathbf{M}_1 \begin{pmatrix} e^{-\gamma L} & 0 \\ 0 & e^{\gamma L} \end{pmatrix} \mathbf{M}_2. \tag{4}$$

Here γ is the complex wave vector of the fundamental propagating TM mode in the MDM waveguide, and L is the distance between the two MDM stub resonators [Fig. 1(a)]. The corresponding transmission and reflection coefficients of the entire system can then be calculated as

$$t = \frac{H_R^-}{H_L^+}\Big|_{H_R^+=0} = \frac{H_L^-}{H_R^+}\Big|_{H_L^+=0} = \frac{b_1 b_2}{-a_1 a_2 e^{-\gamma L} + e^{\gamma L}}, \tag{5}$$

$$r_f = \frac{H_L^-}{H_L^+}\Big|_{H_R^+=0} = \frac{a_2(b_1^2 - a_1^2)e^{-\gamma L} + a_1 e^{\gamma L}}{-a_1 a_2 e^{-\gamma L} + e^{\gamma L}}, \tag{6}$$

and

$$r_b = \frac{H_R^-}{H_R^+}\Big|_{H_L^+=0} = \frac{a_1(b_2^2 - a_2^2)e^{-\gamma L} + a_2 e^{\gamma L}}{-a_1 a_2 e^{-\gamma L} + e^{\gamma L}}. \tag{7}$$

Note that the transmission coefficients for light incident in the forward and backward directions are the same due to reciprocity, whereas the reflection coefficients in the forward (r_f) and backward (r_b) directions are in general different. An exceptional point occurs when the eigenvalues $\lambda_s^{\pm}$ and the corresponding eigenstates $\psi_{\pm}$ coalesce. This in turn happens in the plasmonic system of Fig. 1(a) when the reflection in either the forward or the backward direction is zero. Based on Eqs. (6) and (7), the reflection coefficients in forward and backward directions are

#247970 Received 20 Aug 2015; revised 30 Oct 2015; accepted 3 Nov 2015; published 6 Nov 2015

directly dependent on the lengths of the two MDM stubs L_1 and L_2 [a_i and b_i both depend on the stub lengths based on Eq. (3)] and the distance L between the two MDM stubs. Thus, by properly tuning these geometric parameters, it is possible to obtain an exceptional point which offers an opportunity to control the unidirectional reflection of light in our plasmonic system.

3. Results

In several previous studies, periodic modulation of the refractive index profile, which requires careful tuning of the constituent materials, was used for synthesizing *PT* symmetric optical structures [16–21]. Here, we instead tune the geometric parameters of the proposed structure (Fig. 1) to realize the exceptional point and obtain unidirectional reflectionlessness. The tuning parameters of our proposed structure (Fig. 1) include the lengths of the two MDM stubs L_1, L_2, and the distance L between the two MDM stubs. The width of the MDM waveguide is chosen to be $w = 50$ nm, while the widths of the two MDM stubs are chosen to be $w_1 = 20$ nm and $w_2 = 100$ nm. The metal is chosen to be silver, and the core material of MDM waveguides is air.

We use a two-dimensional finite-difference frequency-domain (FDFD) method [40] to numerically calculate the transmission and reflection coefficients in the MDM plasmonic waveguide structure. This method allows us to directly use experimental data for the frequency-dependent dielectric constant of metals such as silver [41], including both the real and imaginary parts, with no approximation. Perfectly matched layer (PML) absorbing boundary conditions are used at all boundaries of the simulation domain [42].

3.1. Unidirectional reflectionlessness

As mentioned in the previous section, when the two eigenvalues of the scattering matrix **S** [Eq. (1)] are coalesced, the system exhibits an exceptional point, which leads to asymmetric reflection: either the reflection coefficient in the forward direction r_f or the reflection coefficient in the backward direction r_b is zero. If such an asymmetric reflection of light is observed, it reveals the existence of an exceptional point in the optical system. Therefore, here we first design a plasmonic waveguide system with unidirectional reflectionless propagation. The realized exceptional point of the system, as well as the associated physical effects of level repulsion, crossing and phase transition are then investigated in the next Subsection (Subsection 3.2).

To obtain unidirectional reflectionless propagation, we use the scattering matrix theory [Eq. (6)] described in Section 2. More specifically, we optimize the MDM stub lengths L_1, L_2, as well as the distance between the stubs L [Fig. 1(a)], to minimize the amplitude of the reflection coefficient in the forward direction $|r_f|$ at the optical communication wavelength of $\lambda_0 = 1.55\mu$m. The maximum lengths L_1, L_2 and distance L considered in the optimization parameter space are long enough to support at least the second order resonance in each resonator. All complex transmission and reflection coefficients in the scattering matrix equations are numerically extracted using FDFD [35, 43, 44]. Since the MDM waveguide and MDM stubs modes have different field profiles, to extract the product $t_{2i}t_{3i}$ [Figs. 2(a) and 2(b)] we terminate the simulation domain at the plane of both output ports with perfect electric conductor (PEC) boundary conditions [Fig. 2(d)]. Using this approach gives [43, 44]

$$t_{2i}t_{3i} = \frac{r_{3i} - r_{2i}}{2e^{-2\gamma d}\,\frac{1-r_{1i}e^{-2\gamma d}+t_{3i}e^{-2\gamma d}}{(1-r_{1i}e^{-2\gamma d})^2-(t_{1i}e^{-2\gamma d})^2}}, \tag{8}$$

where r_{3i} is the complex reflection coefficient when the fundamental TM mode of a MDM waveguide with width w_i is incident at a junction with a MDM waveguide with width w which is terminated by PEC boundary conditions, and d is the distance from the junction to the PEC

#247970 Received 20 Aug 2015; revised 30 Oct 2015; accepted 3 Nov 2015; published 6 Nov 2015

boundary [Fig. 2(d)]. The scattering matrix model (Section 2) of the structure of Fig. 1(a) is computationally efficient, and thus we are able to use an exhaustive search in the optimization parameter space to minimize the reflection in the forward direction. Using this approach, we find that, the reflection in the forward direction is almost zero ($R_f = |r_f|^2 \simeq 8.18 \times 10^{-9}$) for $L_1 = 175$ nm, $L_2 = 365$ nm, and $L = 561$ nm at $\lambda_0 = 1.55\mu$m. In addition, the reflection in the backward direction for this structure is nonzero ($R_b = |r_b|^2 \simeq 0.619$). Thus, we may conclude that the plasmonic waveguide system of Fig. 1(a) is unidirectional reflectionless, and exhibits an exceptional point for $L_1 = 175$ nm, $L_2 = 365$ nm, and $L = 561$ nm.

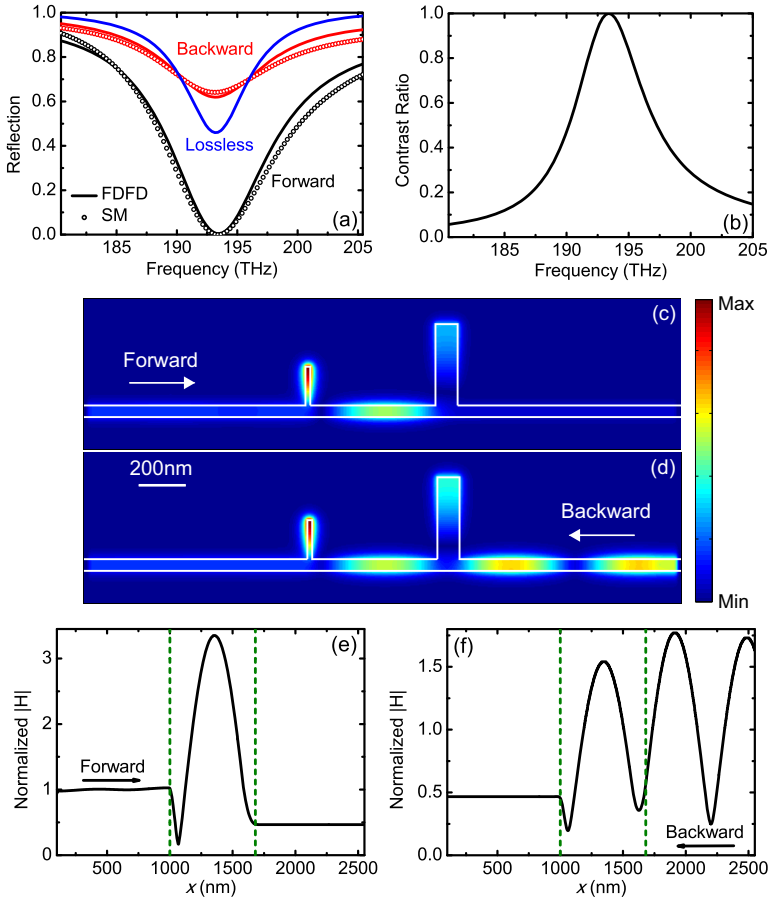

Fig. 3. (a) Reflection spectra for the structure of Fig. 1(a) calculated for both forward and backward directions using FDFD (solid lines) and scattering matrix theory (circles). Results are shown for $w = 50$ nm, $w_1 = 20$ nm, $w_2 = 100$ nm, $L_1 = 175$ nm, $L_2 = 365$ nm, and $L = 561$ nm. Also shown are the reflection spectra calculated using FDFD for lossless metal (blue solid line). (b) Contrast ratio spectra for the structure of Fig. 1(a). All parameters are as in Fig. 3(a). (c) and (d) Magnetic field amplitude profiles for the structure of Fig. 1(a) at f = 193.4 THz ($\lambda_0 = 1.55\mu$m), when the fundamental TM mode of the MDM waveguide is incident from the left and right, respectively. All parameters are as in Fig. 3(a). (e) and (f) Magnetic field amplitude in the middle of the MDM waveguide, normalized with respect to the field amplitude of the incident fundamental TM waveguide mode in the middle of the waveguide, when the mode is incident from the left and right, respectively. The two vertical dashed lines indicate the left boundary of the left stub, and the right boundary of the right stub. All parameters are as in Fig. 3(a).

#247970 Received 20 Aug 2015; revised 30 Oct 2015; accepted 3 Nov 2015; published 6 Nov 2015

Figure 3(a) shows the reflection spectra for the structure of Fig. 1(a) calculated for both forward and backward directions using scattering matrix theory (circles) for $w = 50$ nm, $w_1 = 20$ nm, $w_2 = 100$ nm, $L_1 = 175$ nm, $L_2 = 365$ nm, and $L = 561$ nm. Figure 3(a) also shows the reflection spectra calculated using full-wave FDFD simulations (solid lines). We observe that there is very good agreement between the scattering matrix theory results and the exact results obtained using FDFD. We note that the small off-resonance difference between the scattering matrix theory results and the FDFD results is due to coupling of higher order nonpropagating modes of the waveguides [44]. The effect of the higher order modes is not negligible due to the subwavelength dimensions of the structure. The FDFD results confirm that the optimized structure of Fig. 1(a) is unidirectional reflectionless at $f = 193.4$ THz ($\lambda_0 = 1.55\mu$m). In addition, the contrast ratio between the forward and backward reflection, defined as $\eta = |\frac{R_f - R_b}{R_f + R_b}|$ [20], as a function of frequency is shown in Fig. 3(b). At the wavelength of $\lambda_0 = 1.55\mu$m, the contrast ratio almost reaches unity ($\eta \simeq 0.9999$). The unidirectional reflectionless propagation can be observed in the magnetic field distributions at the exceptional point with $L_1 = 175$ nm, $L_2 = 365$ nm, and $L = 561$ nm [Figs. 3(c)-3(f)]. When the waveguide mode is incident from the right (backward direction), the incident and reflected fields form a strong interference pattern [Figs. 3(d) and 3(f)]. On the other hand, when the waveguide mode is incident from the left (forward direction), there is hardly any reflection [Figs. 3(c) and 3(e)].

We observe that the reflection coefficient in the forward direction r_f becomes zero when $a_2(b_1^2 - a_1^2)e^{-\gamma L} + a_1 e^{\gamma L} = 0$ [Eq. (6)], while the reflection coefficient in the backward direction r_b becomes zero when $a_1(b_2^2 - a_2^2)e^{-\gamma L} + a_2 e^{\gamma L} = 0$. The asymmetric reflection in the plasmonic waveguide system is clearly associated with the different geometrical dimensions of the two stubs, which determine the coefficients a_1, b_1, a_2, and b_2. We also note that, since the reflection in the structure is asymmetric, while the transmission coefficients in the forward and backward directions are the same, the absorption in the structure is also asymmetric. As mentioned above, the width of the left stub w_1 is chosen to be smaller than the width of the right stub w_2, so that the propagation loss per unit length is larger in the left stub. Thus, when the structure of Fig. 1(a) is properly optimized, it is highly absorbing for light incident from the left, while the absorption is low for light incident from the right. We also note that, for light incident from the left, the total reflected wave results from the interference of the wave directly reflected from the left stub, and the decaying amplitude into the backward direction of the resonant cavity fields of the left stub resonator, as well as of the resonator formed between the two stubs. At $f = 193.4$ THz ($\lambda_0 = 1.55\mu$m), these three components interfere destructively, so that the reflection in the forward direction becomes zero.

In most optical devices, the material loss negatively affects the device performance, and as a result the use of lossless transparent dielectric materials is preferred. However, it is worth noting that the unidirectional reflectionless propagation would not be realized in the plasmonic waveguide system of Fig. 1(a), if the material loss in the metal were not present. As mentioned above, the transmission coefficients in the forward and backward directions are always identical due to reciprocity. Thus, in the lossless case the reflection coefficients in the forward and backward directions are also identical, since there is no absorption. When metallic loss is included in the system of Fig. 1(a), the forward reflection is smaller than the one in the lossless case, whereas the backward reflection is larger than the one in the lossless case at f = 193.4 THz [Fig. 3(a)]. In the presence of metallic loss, the plasmonic system is analogous to open quantum systems which are subjected to dissipation and characterized by complex non-Hermitian Hamiltonians [39]. The existence of exceptional points in the system of Fig. 1(a), which is associated with both the eigenvalues and the eigenstates of the scattering matrix coalescing, and which is different from the lossless case, provides an opportunity to control the unidirectional reflection of light. The presence of material loss in turn plays a crucial role on the realization of such a unidi-

#247970 Received 20 Aug 2015; revised 30 Oct 2015; accepted 3 Nov 2015; published 6 Nov 2015

rectional phenomenon in the proposed plasmonic system. This is different from other classical optical analogues of quantum systems, such as the plasmonic analogue of electromagnetically induced transparency [35], which can be realized in both lossless and lossy optical systems.

3.2. *Level repulsion, crossing, and phase transition*

In this subsection, to gain deeper insight into the exceptional point of the system, we investigate the associated phenomena of level repulsion, crossing and phase transition.

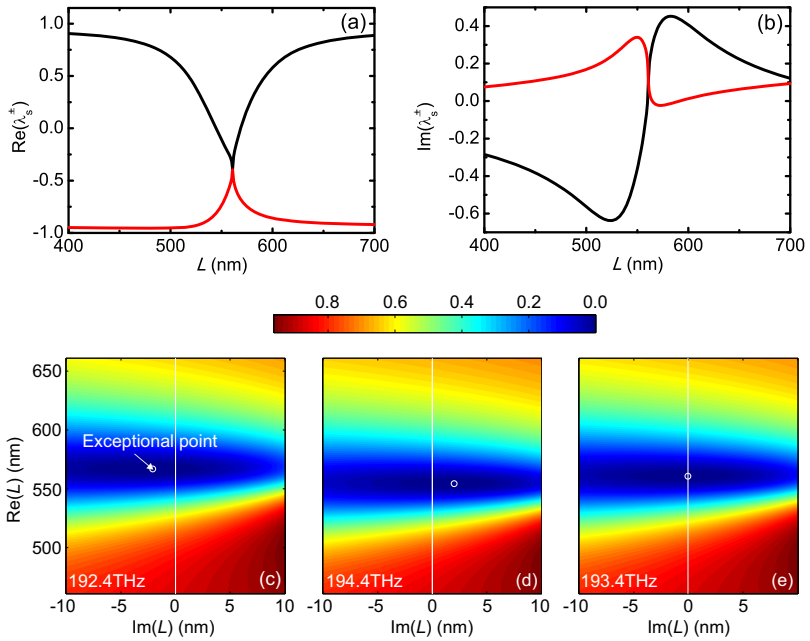

Fig. 4. (a) and (b) Real and imaginary parts of the eigenvalues of the scattering matrix **S** as a function of the distance L between the two MDM stub resonators [Fig. 1(a)]. The black and red lines correspond to eigenvalues $\lambda_s^+ = t + \sqrt{r_f r_b}$ and $\lambda_s^- = t - \sqrt{r_f r_b}$, respectively. All other parameters are as in Fig. 3(a). (c), (d), and (e) Reflection in the forward direction $R_f = |r_f|^2$ as a function of the real and imaginary parts of L at f = 192.4 THz, 194.4 THz, and 193.4 THz, respectively. All other parameters are as in Fig. 3(a). The white circle indicates the location of the exceptional point, and the white vertical line indicates the real L-axis.

In Figs. 4(a) and 4(b) we show the real and imaginary parts, respectively, of the eigenvalues $\lambda_s^{\pm}$ of the scattering matrix **S** [Eq. (1)] as a function of the distance L between the two MDM stub resonators [Fig. 1(a)], calculated using Eqs. (4)-(8) for the optimized plasmonic waveguide structure (Fig. 3). We observe that the real and imaginary parts of the two eigenvalues indeed collapse for L = 561 nm. As discussed above, this is the optimal distance between the two stubs, which minimizes the reflection in the forward direction. Moreover, in open quantum systems, a repulsion (crossing) for the real part of the energy and a crossing (repulsion) for the imaginary part of the energy in the two-dimensional complex energy plane is required around exceptional points [12, 13]. In Figs. 4(a) and 4(b), we indeed observe the level repulsion in the real parts of the eigenvalues, as well as the level crossing in their imaginary parts, which resembles a system consisting of two coupled damped oscillators also described by a non-Hermitian Hamiltonian matrix [12]. Unlike the Hermitian case, the levels approach each other in the form of a cusp

#247970 Received 20 Aug 2015; revised 30 Oct 2015; accepted 3 Nov 2015; published 6 Nov 2015

rather than a smooth approach, because of the plain square root behavior of the singularity [Fig. 4(a)] [12].

To gain further insight into the properties of the exceptional point for the system of Fig. 1(a), we consider the location of the exceptional point, as the distance L between the two MDM stub resonators [Fig. 1(a)] and the frequency f are varied. As we saw above, for f = 193.4 THz ($\lambda_0 = 1.55\mu$m) the exceptional point is located at L = 561 nm [Figs. 4(a) and 4(b)]. We now consider the properties of the system at a slightly lower (f = 192.4 THz), and a slightly higher (f = 194.4 THz) frequency. To locate the exceptional point, we calculate the reflection in the forward direction $R_f = |r_f|^2$ as a function of L. All other geometric parameters of the structure (w, w_1, w_2, L_1, L_2) are fixed as in Fig. 3(a). In this scenario, we find that, if the frequency is varied, no exceptional point occurs if L is purely real. Even though the distance L is a real parameter, here we will allow it to be complex to shed light on the properties of the exceptional point. If the frequency is slightly decreased (f = 192.4 THz), the exceptional point occurs for $L = 567 - j2.1$ nm (the reflection is $R_f = 8.1 \times 10^{-7} \simeq 0$), which is on the left side of the real L-axis [Fig. 4(c)]. If instead the frequency is slightly increased (f = 194.4 THz), the exceptional point occurs for $L = 555 + j2.1$ nm (the reflection is $R_f = 4.4 \times 10^{-7} \simeq 0$), which is on the right side of the real L-axis [Fig. 4(d)]. This suggests that, for a frequency in the interval from 192.4 THz to 194.4 THz, the exceptional point will occur right on the real L-axis. As we have seen before [Figs. 4(a) and 4(b)], at f = 193.4 THz, the exceptional point occurs for $L = 561$ nm, which is indeed purely real [Fig. 4(e)].

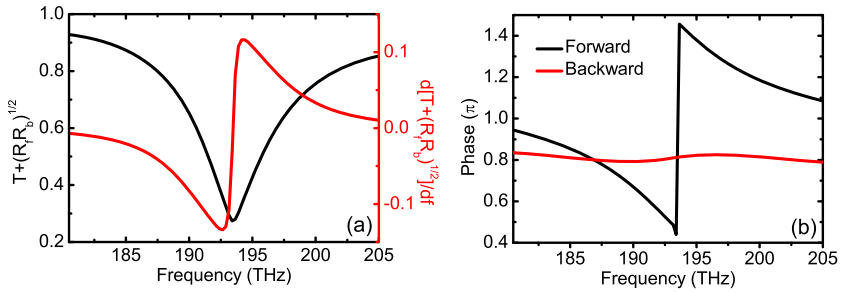

Fig. 5. (a) Spectra of the generalized power $T + \sqrt{R_f R_b}$ (black), and of the differential generalized power (red), defined as the derivative of the generalized power with respect to frequency $d[T + \sqrt{R_f R_b}]/df$, calculated using FDFD. All parameters are as in Fig. 3(a). (b) Phase spectra of the reflection coefficients in the forward (r_f, black) and backward (r_b, red) directions. All parameters are as in Fig. 3(a).

In quantum mechanics, the phase transition due to a non-Hermitian degeneracy is another phenomenon associated with exceptional points [45, 46]. The generalized power representation $T + \sqrt{R_f R_b}$, where $T = |t|^2$ is the transmission, and $R_f = |r_f|^2$ and $R_b = |r_b|^2$ are the reflection in the forward and backward directions, respectively, relates all the elements in the scattering matrix **S**, and is essentially the power summation of superpositions of the two eigenstates [Eq. (1)] [18, 25]. When the reflection in the forward and backward directions are equal, we obtain $T + \sqrt{R_f R_b} = T + R = 1$, which is the power conservation relation for an optical system without gain or loss. In Fig. 5(a), we show the calculated spectra of the generalized power $T + \sqrt{R_f R_b}$ for the structure of Fig. 1(a). Similar to other classical optical systems that have exceptional points [25], we observe that a generalized power decreasing phase, and a generalized power increasing phase are divided by the exceptional point at $f = 193.4$ THz ($\lambda_0 = 1.55\mu$m). In addition, an abrupt phase change in the differential generalized power spectrum is observed at the exceptional point as well [Fig. 5(a)]. These results are due to the fact that the reflection

#247970 Received 20 Aug 2015; revised 30 Oct 2015; accepted 3 Nov 2015; published 6 Nov 2015

coefficient in the forward direction r_f approaches to zero at the exceptional point. We further investigate the phase spectra of the reflection coefficients in the forward (r_f) and backward (r_b) directions [Fig. 5(b)]. We observe that the phase of the reflection coefficient in the forward direction undergoes an abrupt π jump, when the frequency is crossing over the exceptional point, which actually resembles the phase transition from the PT symmetric phase to the PT broken phase in the optical PT-symmetric systems [3, 16-18, 20, 25]. Such an abrupt π phase jump in the reflection coefficient in the forward direction confirms the existence of the exceptional point in the plasmonic system of Fig. 1(a) again, and that the unidirectional reflectionlessness in this system (Subsection 3.1) is directly associated with this exceptional point. In addition, since the refection in the forward direction is zero at the exceptional point, both its real and imaginary parts are zero. This implies that the phase of the reflection coefficient in the forward direction has a singular point, and thus a large phase change around the exceptional point must take place based on the residue theorem [47]. In contrast, the phase of the reflection coefficient in the backward direction does not undergo an abrupt jump, and varies smoothly with frequency [Fig. 5(b)].

3.3. *Unidirectional perfect plasmonic waveguide absorber*

Perfect waveguide absorbers show great promise for switching and interferometric applications in optical circuits [6-8, 28, 48]. Unidirectional perfect absorption may also lead to asymmetric transmission in photonic lattices [49]. Plasmonic slow-light waveguides could be used to realize compact waveguide absorbers, due to the enhanced light-matter interaction in such waveguides, and the decrease of the propagation length of the supported optical mode as the slowdown factor increases [29, 32]. For such applications impedance matching between the input waveguide and the plasmonic slow-light waveguide is required [29].

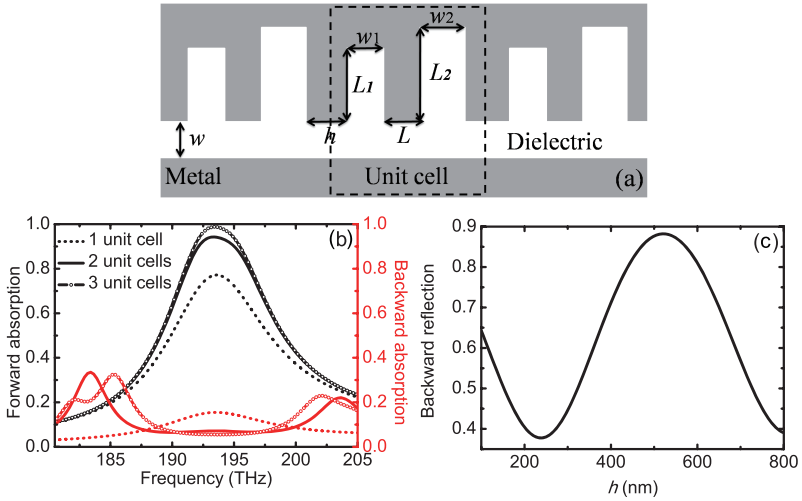

Fig. 6. (a) Schematic of a plasmonic waveguide system consisting of an array of two MDM stub resonators side-coupled to a MDM waveguide. The system is obtained by cascading the side-coupled resonator structure of Fig. 1(a). (b) Absorption spectra for the structure of Fig. 6(a) calculated for both forward (black curves) and backward (red curves) directions using FDFD. Results are shown for $h = 520$ nm for single (dots), double (solid line), and triple (open circles) unit cell structures. All other parameters are as in Fig. 3(a). (c) Reflection in the backward direction as a function of the distance h between two adjacent unit cells for the structure of Fig. 6(a) at $f = 193.4$ THz ($\lambda_0 = 1.55\mu$m). All other parameters are as in Fig. 3(a). Results are shown for the double unit cell structure.

#247970 Received 20 Aug 2015; revised 30 Oct 2015; accepted 3 Nov 2015; published 6 Nov 2015

Achieving zero reflection when light is incident on a structure is a crucial requirement for the realization of total absorption [50]. Here, we design a wavelength-scale unidirectional plasmonic waveguide perfect absorber with complete absorption in the forward direction and almost perfect reflection in the backward direction by periodically cascading [Fig. 6(a)] the unidirectional reflectionless structure of Fig. 1(a). In Fig. 6(b), we show the absorption spectra of the structure of Fig. 6(a) for both forward and backward directions for the single-unit cell structure. The absorption in the forward and backward directions at $f = 193.4$ THz ($\lambda_0 = 1.55\mu$m) are $\sim$77.2% and $\sim$15.5%, respectively. To realize a unidirectional absorber, we wish to simultaneously increase the absorption in the forward direction, as well as decrease the absorption in the backward direction. This will lead to an increase of the contrast ratio between the forward and backward absorption defined as $\eta_A = |\frac{A_f - A_b}{A_f + A_b}|$, where A_f and A_b are the absorption in the forward and backward directions, respectively. Since the transmission in the forward and backward directions are always identical due to reciprocity, in order to maximize the absorption contrast ratio η_A of the waveguide absorber, we need to minimize the transmission. In other words, the ideal structure should exhibit complete absorption in the forward direction and complete reflection in the backward direction.

To increase the absorption contrast ratio η_A, we consider cascading the unidirectional reflectionless structure of Fig. 1(a). Figure 6(c) shows the reflection in the backward direction as a function of the distance h between two adjacent unit cells for the double unit cell structure [Fig. 6(a)]. The maximum backward reflection is obtained for $h = 520$ nm, and is significantly larger than the backward reflection of the single unit cell structure [Fig. 3(a)]. The absorption in the forward and backward directions for the double unit cell structure [Fig. 6(a)] with $h = 520$ nm become $\sim$94.0% and $\sim$7.2%, respectively, at $f = 193.4$ THz ($\lambda_0 = 1.55\mu$m) [Fig. 6(b)]. The absorption in the forward direction further increases to $\sim$99.0%, while the absorption in the backward direction further decreases to $\sim$5.5% for the triple unit cell structure [Fig. 6(b)]. In this case, the absorption contrast ratio η_A reaches $\sim$0.9. In addition, the total length of the triple unit cell structure is $\sim$3.1 μm. In comparison, the required length for a straight MDM waveguide (with width of 50 nm as the structure in Fig. 3) to achieve absorption of $\sim$99.0% is $\sim$55 μm. Thus, the system obtained by cascading the side-coupled resonator structure of Fig. 1(a) is a highly compact unidirectional plasmonic waveguide absorber.

4. Conclusions

In this paper, we designed a non-PT-symmetric plasmonic waveguide-cavity system, consisting of two MDM stub resonators side coupled to a MDM waveguide, to form an exceptional point, and realize unidirectional reflectionlessness at the optical communication wavelength of $\lambda_0 = 1.55\mu$m. The optical properties of the system are described by its scattering matrix which is non-Hermitian. By manipulating the elements of the scattering matrix, its two eigenvalues can be coalesced and form an exceptional point. This leads to unidirectional reflectionless propagation in either the forward or the backward direction.

We used single-mode scattering matrix theory to account for the behavior of the system. To obtain unidirectional reflectionless propagation, we used the scattering matrix model, and optimized the geometric parameters of the structure, to minimize the reflection in the forward direction at the optical communication wavelength. Using this approach, we found that for the optimized structure the reflection in the forward direction is almost zero, while the reflection in the backward direction is nonzero. Thus, such a plasmonic waveguide system is unidirectional reflectionless, as also confirmed by full-wave FDFD simulations. In addition, the contrast ratio between the forward and backward reflection almost reaches unity. We found that the presence of material loss in the metal is critical for the realization of the unidirectional reflectionlessness in this plasmonic system.

#247970 Received 20 Aug 2015; revised 30 Oct 2015; accepted 3 Nov 2015; published 6 Nov 2015

We then investigated the realized exceptional point of the system, as well as the associated physical effects of level repulsion, crossing and phase transition. We found that the real and imaginary parts of the two eigenvalues of the system collapse for the optimized parameters. We also observed level repulsion in the real parts of the eigenvalues, as well as level crossing in their imaginary parts, which resembles open quantum systems. In addition, we observed that the phase of the reflection coefficient in the forward direction undergoes an abrupt π jump, when the frequency is crossing over the exceptional point, which resembles the phase transition from the *PT*-symmetric phase to the *PT*-broken phase in optical *PT*-symmetric systems.

Finally, we designed a wavelength-scale unidirectional plasmonic waveguide perfect absorber with complete absorption in the forward direction and almost perfect reflection in the backward direction by periodically cascading the unidirectional reflectionless plasmonic waveguide-cavity system. Our results could be potentially important for developing a new generation of highly compact unidirectional integrated nanoplasmonic devices.

As final remarks, we note that the formation of an exceptional point and the resulting unidirectional reflectionlessness can also be realized in similar plasmonic waveguide-cavity systems based on other plasmonic two-conductor waveguides, such as three-dimensional plasmonic coaxial waveguides [51, 52].

Acknowledgments

Y. H. acknowledges the support of the Postdoctoral Research Foundation of CSU. G.V. acknowledges the support of the National Science Foundation (Awards No. 1102301 and 1254934). C. M. acknowledges the support given by National Natural Science Foundation of China under Grant numbers 61422506 and 11204141.

#247970 Received 20 Aug 2015; revised 30 Oct 2015; accepted 3 Nov 2015; published 6 Nov 2015